Proceedings of the 11th World Congress on Mechanical, Chemical, and Material Engineering (MCM'25)

Paris, France - August, 2025 Paper No. HTFF 179 DOI: 10.11159/htff25.179

Preliminary CFD Analysis on the Effects of Conjugate Problems for a Smooth Duct and a Kagome Lattice Channel: Average Results for Heat Transfer and Pressure Losses

Giacomo Tosatti¹, Sandra Corasaniti¹, Michele Potenza¹, Ivano Petracci^{1,*}

¹Department of Industrial Engineering, University of Rome "Tor Vergata", via del Politecnico n.1, 00133 Rome, Italy giacomo.tosatti@alumni.uniroma2.eu; sandra.corasaniti@uniroma2.it, michele.potenza@uniroma2.it, ivano.petracci@uniroma2.it (*corresponding author)

Abstract – The compactness of electronic devices and mechanical components and the constant increase in power density pose significant challenges in thermal management. These geometric constraints imply the reduced length of the channels dedicated to their cooling, hence the need to properly analyze the conjugate heat transfer problem and develop new innovative heat dissipation systems, such as lattice structures. This paper aims to numerically investigate the thermo-fluid dynamics properties of a short empty duct 80 mm long, named K0, with a cross-section of 15x5 mm in two different flow conditions: fully developed and developing flow. Then, the same channel is equipped with a Kagome-truss lattice with a truss diameter of 0.8 mm, named K1 and characterized by a porosity ϕ =87%, and the analysis is repeated for both outflow conditions. The thermal fluid is air, and the operating Reynolds numbers range from 2852 to 17115 for all the studied cases, thus falling within the transitional flow regime. Results for the smooth duct show its sensitivity to flow conditions, revealing a substantial increase in the Nusselt number by up to 13% at the cost of a higher friction factor, as is expected from existing studies in the literature. On the contrary, no significant variation in friction factor and Nusselt number is observed for the K1, suggesting that its thermo-fluid dynamic properties are more influenced by the lattice structure rather than the flow profile. Finally, the two ducts are compared in terms of energy efficiency, evaluated as Nu/ λ 1/3, revealing that at the same Reynolds number, the efficiency of the Kagome duct is up to 2.2 and 2.4 times greater than that of the empty duct in fully developed and developing flow condition respectively.

Keywords: RANS Numerical Simulations; Conjugate Entry Length Problem; Kagome Lattice Channel; Smooth Duct; Porous Media; Convective Heat Transfer; Pressure Losses

1. Introduction

In industrial design, some of the most critical challenges include geometric and spatial constraints, such as those encountered in compact heat exchangers. These constraints result in a limited length of the cooling channels. Hence, the comprehension of the conjugate problem, which involves the simultaneous development of both the hydrodynamic and thermal boundary layers, becomes critical. Furthermore, since the flow is not fully developed, the range of Reynolds numbers that determine its regime is significantly affected and often falls within the transitional regime, a condition which has been experimentally studied by a wide range of researchers such as Gnielinski [1], Churchill [2] and Tam and Ghajar [3].

These limitations, combined with the need to dissipate an ever growing thermal power to ensure the correct functionality and preservation of mechanical and electronic components, have driven scientific research toward developing innovative heat dissipation systems. Porous and periodic cellular materials (PCM) are highly promising multifunctional materials, with broad applications ranging from the aerospace and automotive sectors [4] to energy storage and heat transfer systems [5]. Among PCMs, truss based PCMs carved out a prominent spot due to their superior structural resistance to both static and dynamic loads [6] and their heat dissipation capability, which can reach values up to seven times higher than that of an empty channel with a lower pressure drop compared to other non-truss based options, leading to a thermal efficiency that outperforms typical heat sinks media such as pin fins and cylinder banks [7]. Among truss-based lattices, the Kagome type exhibits isotropic mechanical responses under compression and shear, and unlike tetragonal PCMs, this behaviour remains unchanged after yielding [8]. Moreover, Kagome lattices provide a higher heat dissipation rate, up to 38%, for a fixed pumping power compared to the tetragonal counterpart, reaching values comparable to the X-type lattice [9]. For this reasons, several additional studies have been conducted in order to optimize the Kagome performances further. Joo et al. [10] investigated the heat transfer capabilities of wire-woven bulk Kagome (WBK) made of aluminum helix wires in forced

convection, analyzing the effect of Kagome orientation as well by altering the flow pattern. The results showed that the "most closed" orientation possesses a considerably higher Nusselt number for each tested flow rate at the cost of a slightly increased pressure drop. However, Shen et al. [11] found that the truss-cored Kagome achieves an overall Nusselt number up to 26% higher than a WBK, while maintaining a similar pressure drop. This is because a large portion of the ligaments is near the walls of the employed sandwich panels and so the flow blockage increases, leading to the formation of low-momentum vortices.

This research group previously conducted various experimental studies on an X-type lattice structure to evaluate its thermal and fluid dynamic performances under different flow regimes and working fluids [12], [13]. This work aims to lay the groundwork for a future experimental campaign on a newly designed lattice structure and, to achieve this goal, a series of 3D RANS numerical simulations of the pressure drop, heat dissipation capability and thus thermal efficiency of a short smooth duct, namely K0, in which the working fluid is air, under two different flow conditions: fully developed flow and a flat inlet velocity profile, thereby accounting for inlet and outlet effects. Subsequently, the same analysis will be repeated on a duct equipped with the Kagome lattice, labelled K1, featuring a cell staggering equal to half the characteristic cell size in the transition from the first to the second row, which is repeated periodically along the whole duct. The total porosity ϕ of the channel, defined as the ratio of the void to the entire internal volume, is equal to 87%. Results highlight the net enhancement of the aforementioned key parameters and, thus, the advantages of using these thermal dissipation media in systems with high heat generation rates.

2. Numerical methodology

2.1. Governing equations

The governing equations of the problem in exam are the three Navier-Stokes equations, namely the conservation of mass, momentum and energy. Assuming the fluid to be incompressible they can be written as shown in Eqs. (1) - (3):

$$\frac{\partial u_i}{\partial x} = 0 \tag{1}$$

$$\frac{\partial u_{i}}{\partial x_{i}} = 0$$

$$\frac{\partial u_{i}}{\partial t} + u_{j} \frac{\partial u_{j}}{\partial x_{j}} = -\frac{1}{\rho} \frac{\partial p}{\partial x_{i}} + v_{j} \frac{\partial^{2} u_{i}}{\partial x_{j} \partial x_{j}}$$

$$\frac{\partial T}{\partial t} + u_{j} \frac{\partial T}{\partial x_{i}} = \alpha \frac{\partial T^{2}}{\partial x_{j} \partial x_{j}}$$
(2)
$$(3)$$

$$\frac{\partial T}{\partial t} + u_j \frac{\partial T}{\partial x_j} = \alpha \frac{\partial T^2}{\partial x_j \partial x_j}$$
(3)

Indeed, a direct approach to directly solve these equations would be impractical, hence the choice to adopt a RANS approach, decomposing the flow variables of the three equations as shown in Eq. (4) for velocity:

$$u_{i} = \bar{u}_{i} + u_{i}^{'} \tag{4}$$

Where u_i is the time-averaged quantity and u_i the fluctuating term. By substituting the decomposed variables back in the instantaneous form of the Navier Stokes equations, the time averaged are obtained as follows in Eqs. (5) - (7).

$$\frac{\partial U_i}{\partial x_i} = 0 \tag{5}$$

$$\frac{\partial U_{i}}{\partial x_{i}} = 0$$

$$\frac{\partial U_{i}}{\partial x_{i}} + U_{j} \frac{\partial U_{j}}{\partial x_{j}} = -\frac{1}{\rho} \frac{\partial P}{\partial x_{i}} + \frac{\partial}{\partial x_{j}} \left(\nu \frac{\partial U_{j}}{\partial x_{j}} - \overline{u_{i}} \overline{u_{j}} \right)$$
(6)

$$\frac{\partial T}{\partial t} + U_{j} \frac{\partial T}{\partial x_{j}} = \frac{\partial}{\partial x_{j}} \left[k \frac{\partial T}{\partial x_{j}} - T' u_{j}' + \frac{\mu}{\rho c} \left(\frac{\partial U_{j}}{\partial x_{j}} \right) \right]$$
(7)

The overbarred terms $\overline{u_{i}^{'}u_{j}^{'}}$ and $T^{'}u_{j}^{'}$ are the Reynolds stresses tensor and turbulent heat flux respectively. These terms describe the influence of the instantaneous components on the mean flow field and, according to the Boussinesq' hypothesis, they are modelled as:

 $-\overrightarrow{u_i}\overrightarrow{u_j} = \nu_t \left(\frac{\partial u_i}{\partial x_j} + \frac{\partial u_j}{\partial x_j}\right) - \frac{2}{3} \left(k + \nu_t \frac{\partial u_i}{\partial i}\right) \delta_{xj}$ $k = \frac{1}{2} \left(\overline{u_1^2} + \overline{u_2^2} + \overline{u_3^2}\right)$ (5)

$$k = \frac{1}{2} \left(\overline{u_1^2} + \overline{u_2^2} + \overline{u_3^2} \right) \tag{6}$$

$$-\overline{Tu_{j}} = k_{t} \frac{\partial T}{\partial x_{j}}$$

$$(7)$$

Where v_t is the eddy kinematic viscosity, k_t the turbulent thermal conductivity, k the turbulent kinetic energy. The problem is then reduced to the sole determination of the unknown variable ν_p , which is modelled with two auxiliary equations in the so called two equations turbulence models. In the present work the k- ω SST by Menter [14] is employed, combining the $k-\omega$ formulation in the innermost part of the boundary layer (i.e. near walls) in order to correctly solve the strong gradients, and the robustness of the k- ε model in the free-stream. The equations for k and ω are as follows:

$$\frac{\partial k}{\partial t} + u_{j} \frac{\partial k}{\partial x_{i}} = \frac{\partial}{\partial x_{i}} \left[\left(\nu + \sigma^{*} \frac{k}{\omega} \right) \frac{\partial k}{\partial x_{i}} \right] + \overrightarrow{u_{i}} \overrightarrow{u_{j}} \frac{\partial u_{i}}{\partial x_{i}} - \beta^{*} k \omega$$
(8)

$$\frac{\partial \omega}{\partial t} + u_j \frac{\partial \omega}{\partial x_j} = \frac{\partial}{\partial x_j} \left[\left(\nu + \sigma \frac{k}{\omega} \right) \frac{\partial \omega}{\partial x_j} \right] + \frac{\alpha \omega}{k} u_i u_j \frac{\partial u_i}{\partial x_j} - \beta k \omega + \frac{\sigma_d \partial \omega \partial k}{\omega \partial x_j \partial x_j}$$

$$\tag{9}$$

More details on the variables and constants of the equations mentioned above can be found in [15]. It should be noted that, in the present work, all time derivatives are identically zero, as the problem is studied under steady state conditions.

2.2. Grid generation

As mentioned in the abstract and in the introduction section, two different types of ducts are considered. The first one is a smooth aluminium channel 80 mm long with a flow cross-section of 15 mm by 5 mm, while the mantle's thickness is set to 0.7 mm. An additional 35 mm long duct is added after the heated channel to avoid any type of outlet-influence on the velocity gradients and, thus, on the heat transfer mechanism. A structured mesh is employed, given the simplicity of the studied geometry, with the fluid discretized with a single block, while the solid with five. The 15 mm side needed 90 nodes while the shorter side only 40 to guarantee a y⁺ <1 and a growth ratio equal to 1.15 utilizing a bigeometric growth law. Then, one element per millimeter of the channel's length is employed to discretize the streamwise direction.

The boundary conditions, as well as a detail of the symmetry plane and cross-section are shown in Fig. 1. A velocity inlet boundary condition, colored in red, is applied at the start of the domain, while a pressure outlet with a gauge pressure equal to 0 Pa is imposed on the far end, as shown by the cyan surface. Six different volumetric flow rates are tested, from 25 l/min to 150 l/min in steps of 25. A uniform heat flux q'' equal to 13700 W/m² is applied on the channel's outer mantle, colored in light green. The internal walls of the channel are treated as no-slip walls: the blue wall is considered to be diabatic, while the orange one is adiabatic. The solid's transverse boundaries, colored in grey, are treated as diabatic walls. Given the symmetry of the domain, only half of it is modelled; however, the symmetry plane is not reported in Fig.1 for clarity purposes.

As far as the inlet condition is concerned, in the fully developed flow case, an additional simulation in a very long duct (20 times the length reported above) for each flow rate was performed in order to ensure an appropriate entry length for the fluid, thus obtaining a fully developed profile for the velocity field and the turbulent transport quantities (i.e. k and ω), which are then used as entry conditions. In contrast, velocities are constant in the developing flow case, hence a flat velocity profile is applied. The turbulent kinetic energy and dissipation rate are carefully set to match the average values of their counterparts in the first case.

A representation of the Kagome lattice can be found in Fig. 2. The base cell is modelled in its entirety in the first row, with offset equal to half its characteristic length in the second row. The lattice then repeats itself periodically for the 80 mm length of the channel.

An extra section 35 mm long was added after the inlet section, contrary to the smooth case, to avoid convergence issues during the simulation. A fully unstructured poly-hexa mesh was employed to lower the total element count and minimize numerical diffusion compared to tetrahedral elements. The first cell height is set to obtain a $y^+<1$ and 13 layers are grown from each wall with a last-ratio approach to guarantee a growth ratio equal to 1.15 and a smooth transition to the hexa volume mesh. The boundary conditions remained unchanged, the lattice was treated as a no-slip diabatic wall. A closeup of the surface mesh on the symmetry plane can be found in Fig.3a, while a detail of the volume mesh can be appreciated in Fig.3b.

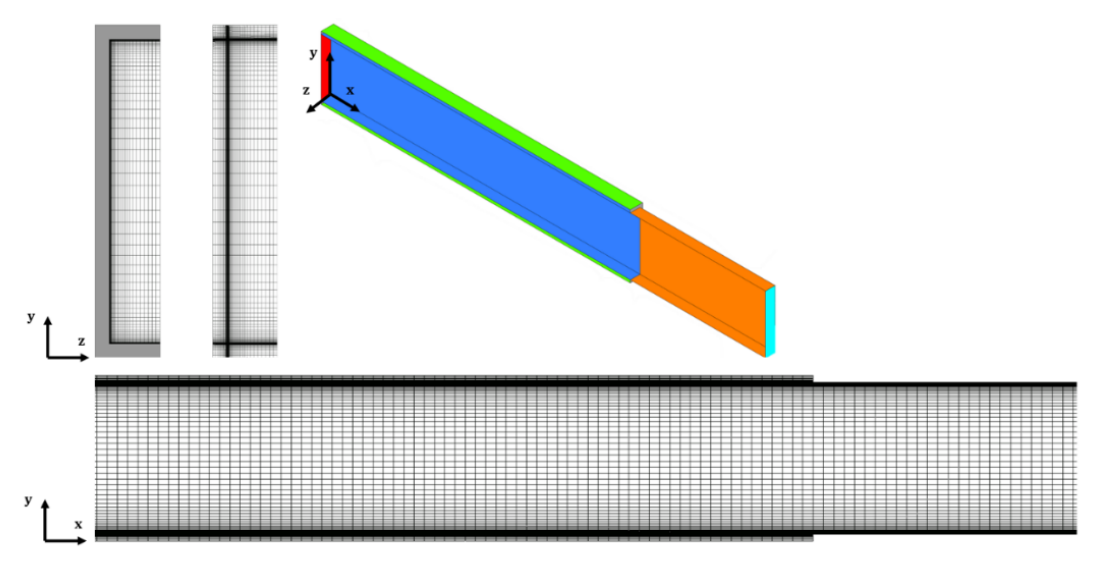


Fig. 1: Side and front view of the meshed smooth duct, along with isometric view of all domain.

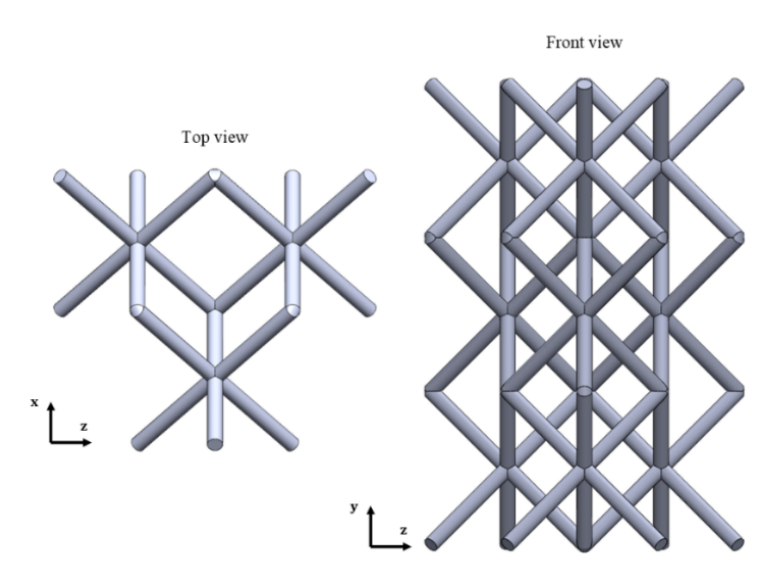


Fig. 2: Top and front view of the first two rows of the Kagome lattice.

The equation of momentum, energy, pressure, TKE and specific dissipation were discretized with a second order upwind scheme and the simulations were considered converged when every residual reached a value of 10⁻¹⁰ for the smooth pipe, which was accomplished under 500 iterations, and 10⁻⁶ for the Kagome case.

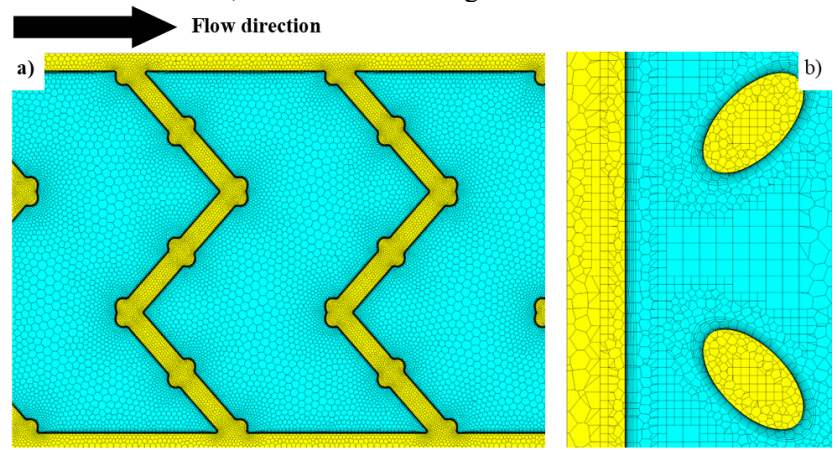


Fig. 3: Employed poly-hexa mesh. a) Surface mesh on symmetry plane. b) Volume mesh.

3. Results

3.1. Mesh validation

Six different flow rates have been simulated and results were compared in terms of friction factor λ and Nusselt number Nu, whose equations are reported in Eqs. (10)-(11) respectively, to famous works in open literature. In particular, the convergence and mesh independence study for the K0 duct was conducted for the fully developed flow case, comparing the results to the Blasius and Dittus-Boelter correlations, which can be found in Eqs. (12)-(13).

$$A = \frac{2\Delta P D_{idr}}{a \ln^2} \tag{10}$$

$$\lambda = \frac{2\Delta PD_{idr}}{\rho L w^2}$$

$$Nu = \frac{hD_{idr}}{k}; h = \frac{q''}{(T_{wall} - T_{bulk})}$$

$$\lambda_{Blasius} = \frac{0.316}{Re_{D_{idr}}^{0.25}}$$
(12)

$$\lambda_{Blasius} = \frac{0.316}{Re_{D_{idr}}^{0.25}} \tag{12}$$

$$Nu_{Dittus-Boelter} = 0.023 Re_{D_{idr}}^{0.8} Pr^{0.4}$$
(13)

The thermophysical properties of the air were considered constant and evaluated at the inlet temperature of 20°C, the mass-average of pressure drop and bulk temperature were considered when estimating the convective heat transfer coefficient h in Eqs. (10)-(11) respectively.

Tab. 1 provides an overview of the simulations, while Fig. 4 compares the friction factor and Nusselt number to Blasius' and Dittus-Boelter's correlations. Results are deemed satisfactory, therefore the previously described mesh was chosen to extend the investigation to the developing flow profile.

Three different meshes were studied for the Kagome K1 duct, generated by varying the number of hexahedral elements, while keeping the number of inflation layers unchanged. The total element count amounts to 5.5, 7.8 and 11 million fluid elements for the coarse, medium and fine grids, respectively. Tab.2 shows results of the analysis in terms of friction factor and Nusselt number for the three tested grids, obtained for a volumetric flow rate of 150 l/min. Since the percentage difference from the medium to the fine mesh is 0.47% for λ and 0.33% for Nu, the medium grid has been utilized to carry on the simulations.

$V\left[\frac{l}{min}\right]$	$w\left[\frac{m}{s}\right]$	Re _{Didr}		
25	5.55	2852		
50	11.11	5704		
75	16.66	8557		
100	22.22	11410		
125	27.77	14262		
150	33.33	17115		

Tab. 1: Volumetric flow rates, corresponding velocities and Reynolds number

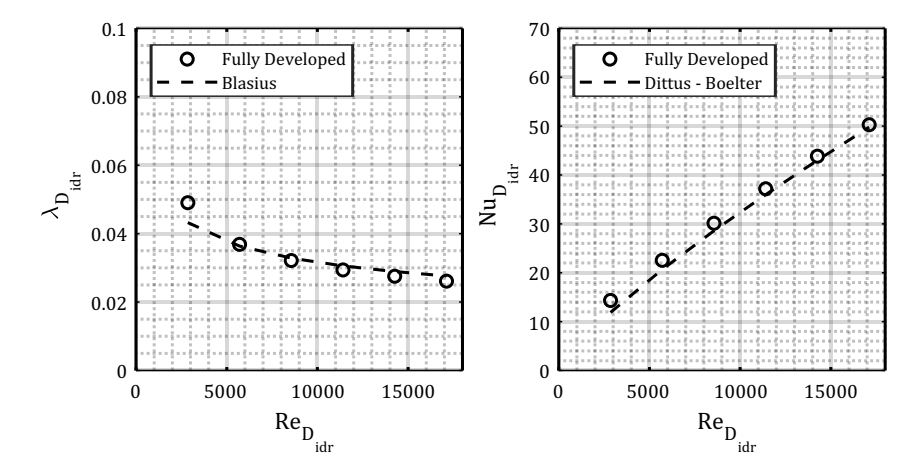


Fig. 4: Numerical results for the K0 duct in fully developed flow condition and comparison with correlations from literature.

N° elements	λ_{Didr}	Nu _{Didr}	Δλ _{Didr} [%]	ΔNu _{Didr} [%]
$5.5 \cdot 10^6$	1.592	264.40	/	/
$7.8 \cdot 10^6$	1.637	277.38	2.73%	4.90%
$11 \cdot 10^6$	1.629	278.29	0.47%	0.33%

Tab. 2: Mesh independency study; parameters and output.

3.2. Pressure Drop and Heat Transfer

Lastly, a thorough comparison between all the proposed tested cases is presented in the following figures. Fig. 5 shows the friction factor and Nusselt number trends for the K0 pipe for both flow conditions. As expected, the flat velocity profile increases the friction factor due to the higher wall shear. Moreover, the resulting temperature profile exhibits a gradient that enhances heat transfer, leading to a higher Nusselt number. This result is compared with the Gnielinski correlation [1], highlighting the reliability of the obtained data. The same analysis is repeated for the K1 duct and reported in Fig. 6, in which it is possible to observe the independence of heat transfer from the flow condition, although a slight influence on the friction factor can still be noted. This suggests that the shape and arrangement of the lattice determine its heat transfer characteristics,

not the entry length. Finally, Fig. 6 also highlights the thermal efficiency ε of the two pipes, obtained from dimensional analysis as in Eq. (14):

$$Q \sim \Delta PwL^3$$
 $\lambda \sim \frac{\Delta P}{w^2}$ $Re_{Didr} \sim wL$ $Q \sim \lambda Re_{D_{idr}}^3$ $\varepsilon \sim \frac{Nu_{D_{idr}}}{\frac{1}{3}}$ (14)

where Q is the pumping power. From this figure, the advantage of the K1 channel over its smooth counterpart is clearly evident, as efficiencies up to 2.2 times higher can be achieved in the case of fully developed flow, and 2.4 times greater for the developing flow.

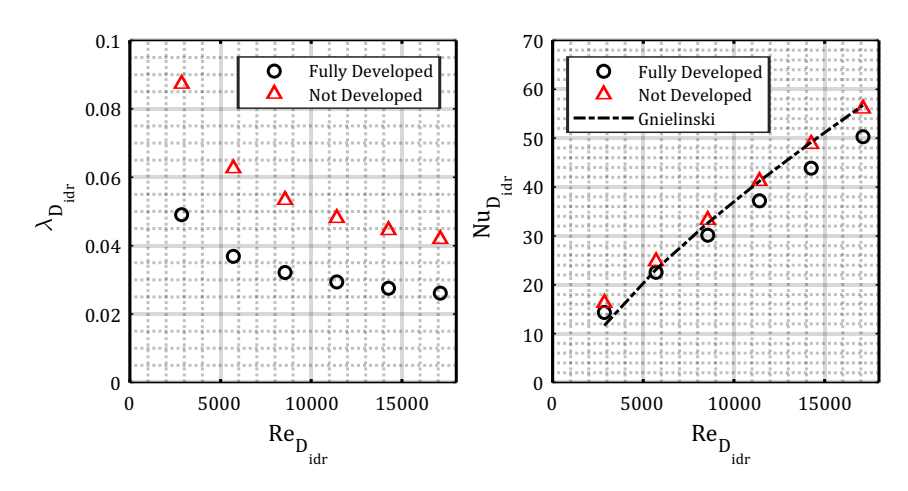


Fig. 5: Comparison between the fully developed and developing flow cases, K0 duct.

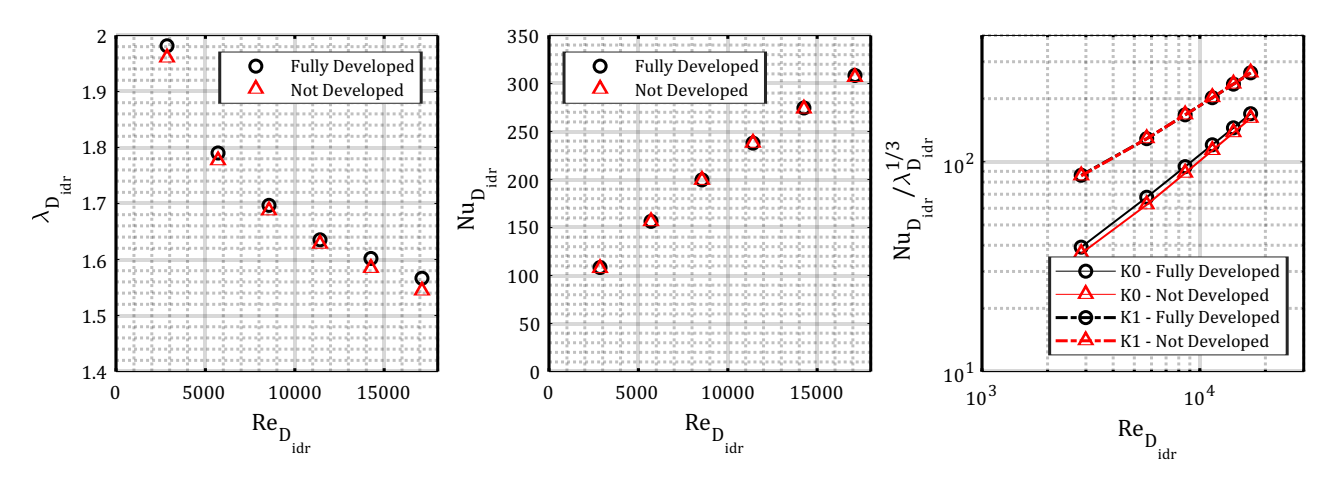


Fig. 6: Comparison between the fully developed and developing flow cases, K1 duct. Thermal efficiency of the two channels as a function of Reynolds number.

4. Conclusion

A series of 3D RANS simulations was conducted on an empty rectangular-section channel, K0, for two different inflow conditions: fully developed and flat velocity profiles. The same analysis was then repeated on the

channel equipped with a Kagome lattice, K1. The results for the smooth channel demonstrated its sensitivity to the velocity profile, with a noticeable increase of the Nusselt number up to 13%. However, this is followed by a greater pressure drop, leading to a lower thermal efficiency for every tested flow regime. The K1 duct showed no significant difference between the two inlet conditions, suggesting that the lattice arrangement along the duct primarily influences its heat dissipation capabilities. Lastly, the K1 channel showed far greater thermal efficiency for each Reynolds number and each flow condition, reaching peak values up to 2.4 times the baseline case.

References

[4]

- [1] V. Gnielinski, "New Equations for Heat and Mass Transfer in Turbulent Pipe and Channel Flow," *Int. Chem. Eng.*, vol. 16, pp. 359–368, 1976.
- [2] S. W. Churchill, "Comprehensive Correlating Equations for Heat, Mass and Momentum Transfer in Fully Developed Flow in Tubes," *Ind. Eng. Chem. Fundam.*, vol. 16, no. 1, pp. 109–116, 1977.
- [3] L. M. Tam, "Transitional heat transfer in plain horizontal tubes," in *Heat Transfer Engineering*, Jun. 2006, pp. 23–38. doi: 10.1080/01457630600559538.
 - N. Khan and A. Riccio, "A systematic review of design for additive manufacturing of aerospace lattice structures: Current trends and future directions," Aug. 01, 2024, *Elsevier Ltd.* doi: 10.1016/j.paerosci.2024.101021.
- [5] S. A. Khan, M. A. Rahman, M. Khraisheh, and I. G. Hassan, "Advances in 3D printed periodic lattice structures for energy research: Energy storage, transport and conversion applications," Mar. 01, 2024, *Elsevier Ltd.* doi: 10.1016/j.matdes.2024.112773.
- [6] H. N. G. Wadley, "Multifunctional periodic cellular metals," *Philosophical Transactions of the Royal Society A: Mathematical, Physical and Engineering Sciences*, vol. 364, no. 1838, 2006, doi: 10.1098/rsta.2005.1697.
- [7] T. Kim, C. Y. Zhao, T. J. Lu, and H. P. Hodson, "Convective heat dissipation with lattice-frame materials," in *Mechanics of Materials*, 2004. doi: 10.1016/j.mechmat.2003.07.001.
- [8] S. Hyun, A. M. Karlsson, S. Torquato, and A. G. Evans, "Simulated properties of Kagomé and tetragonal truss core panels," *Int J Solids Struct*, vol. 40, no. 25, pp. 6989–6998, 2003, doi: 10.1016/S0020-7683(03)00350-0.
- [9] H. B. Yan, Q. C. Zhang, T. J. Lu, and T. Kim, "A lightweight X-type metallic lattice in single-phase forced convection," *Int J Heat Mass Transf*, vol. 83, 2015, doi: 10.1016/j.ijheatmasstransfer.2014.11.061.
- [10] J. H. Joo, K. J. Kang, T. Kim, and T. J. Lu, "Forced convective heat transfer in all metallic wire-woven bulk Kagome sandwich panels," *Int J Heat Mass Transf*, vol. 54, no. 25–26, 2011, doi: 10.1016/j.ijheatmasstransfer.2011.08.018.
- [11] B. Shen, H. Yan, H. Xue, and G. Xie, "The effects of geometrical topology on fluid flow and thermal performance in Kagome cored sandwich panels," *Appl Therm Eng*, vol. 142, 2018, doi: 10.1016/j.applthermaleng.2018.06.080.
- [12] S. Corasaniti, M. Potenza, and I. Petracci, "Preliminary Results of Heat Transfer and Pressure Drop Measurements on Al2O3/H2O Nanofluids through a Lattice Channel," *Energies (Basel)*, vol. 16, no. 9, 2023, doi: 10.3390/en16093835.
- [13] I. Petracci, S. Corasaniti, M. Potenza, G. Tosatti, D. Santoro, and L. Consolini, "Thermo-fluid dynamic behaviour of a small length 3D printed lattice channel in a conjugated problem," *Int J Heat Mass Transf*, vol. 240, May 2025, doi: 10.1016/j.ijheatmasstransfer.2024.126644.
- [14] F. R. Menter, "Two-equation eddy-viscosity turbulence models for engineering applications," *AIAA Journal*, vol. 32, no. 8, 1994, doi: 10.2514/3.12149.
 - [15] D. C. Wilcox, "Reassessment of the scale-determining equation for advanced turbulence models," *AIAA Journal*, vol. 26, no. 11, 1988, doi: 10.2514/3.10041.